Applied Thermal Engineering 161 (2019) 114144

Contents lists available at ScienceDirect

Applied Thermal Engineering

journal homepage: www.elsevier.com/locate/apthermeng

Research Paper

Study on thermal stability of nickel-rich/silicon-graphite large capacity lithium ion battery

Hang Li, Xiangbang Kong, Chaoyue Liu, Jinbao Zhao*

State Key Lab of Physical Chemistry of Solid Surfaces, Collaborative Innovation Centre of Chemistry for Energy Materials, State-Province Joint Engineering Laboratory of Power Source Technology for New Energy Vehicle, Engineering Research Center of Electrochemical Technology, Ministry of Education, College of Chemistry and Chemical Engineering, Xiamen University, Xiamen 361005, PR China

HIGHLIGHTS

- The changes of the thermal stability of the battery with different charge state was observed in DSC and ARC data.
- The thermal stability mutation of Si@C material has been observed.
- The thermal stability of NMC811/Si@C metrical was deeply researched, a reasonable thermal runaway sequence was proposed.
- Based on ARC data, the TMR curve is predicted, which can provide guidance on the safe use of the NMC811/Si@C battery.

ARTICLE INFO

Keywords:
High energy density battery
Power lithium-ion battery
Thermal stability
Differential scanning calorimetry
Adiabatic rate calorimetry
Thermal runaway prediction

ABSTRACT

The nickel-rich silicon-graphite lithium-ion cells, for example the $LiNi_{0.8}Mn_{0.1}Co_{0.1}O_2$/Silicon-carbon (NMC811/Si@C), have been used in the commercial power batteries to meet the higher capacity requirements now. However, the battery with higher energy is more destructive as thermal runaway occurs. In order to improve the safety of the battery, it is essential to study the thermal stability of this kind of battery. In this work, the differential scanning calorimetry (DSC) and adiabatic rate calorimetry (ARC) have been used to conduct a detail thermal stability analysis for this type of battery of different charge state, the thermal stability mutation of Si@C material has been observed firstly when the SOC is great than 55%. Besides, a reasonable thermal runaway reaction sequence of the battery of NMC811/Si@C is proposed. Moreover, based on the time to maximum reaction rate (TMR), the effective recommendations for the use of NMC811/Si@C lithium ion battery are provided.

1. Introduction

The lithium ion battery is considered to be a kind of clean energy with higher energy density, longer cycle life, no pollution and no memory effect. It is widely used in the communication, transportation and other industries around the world [1,2]. With the popularity of lithium ion battery continues to increase, especially electric vehicles, in order to make the battery working hours longer, the demand for lithium-ion batteries with higher energy density will be even more urgent [3,4].

In order to provide higher energy, the silicon-carbon material has been used as an anode material, which has a higher capacity (over 400 $mAh{\cdot}g^{-1}$ [5–7]) than the traditional graphite material (372 $mAh{\cdot}g^{-1}$) [7,8]. At the same time, to match the capacity of the anode electrode, the layered transition metal oxide, $LiNi_{0.8}Mn_{0.1}Co_{0.1}O_2$ (NMC811), has been applied as the cathode material, which has a capacity of 275.5 $mAh{\cdot}g^{-1}$ [9,10]. Because this type of battery with such system have been used in the commercial applications, the research on the thermal stability of this type battery is very important.

The cathode electrode material NMC undergoes a lattice transition under high temperature conditions while oxygen is released. The oxygen will easily reacts with the electrolyte inside the battery and the lithium-intercalated anode material, which may easily cause thermal runaway of the battery [11–14]. Bak et al. [15] conducted thermal stability analysis of charged $LiNi_xMn_yCo_zO_2$ ($x + y + z = 1$) by *in-situ* time-resolved X-ray diffractometer (XRD) and mass spectroscopy, and considered that the onset temperature of thermal decomposition of NMC materials decrease as the increase of Ni content and decrease of Co/Mn content. Belharouak et al. [16] used the DSC and XRD to study

* Corresponding author.
E-mail address: jbzhao@xmu.edu.cn (J. Zhao).

https://doi.org/10.1016/j.applthermaleng.2019.114144
Received 20 May 2019; Received in revised form 16 July 2019; Accepted 16 July 2019
Available online 17 July 2019

the NMC111, and found that the material will become more stable when the phase change from $R\bar{3}m$ layered phase to $Fd3m$ spinel phase. In addition, the Si@C anode electrode material also has corresponding safety problems. It is widely known that Si will undergo a nearly 400% volume change during charging [6,17–19]. A large volume change in charging process will increase the internal stress of the battery [5]. The strong internal stress generated by the volume change may lead to the cracking and pulverization of Si@C anode electrode [20–23], and the rupture of separator, followed by partial short circuits and even thermal runaway [3,17]. Besides, the capacity fade of lithium-ion batteries with silicon-based anodes is also related to the volume change of Si@C of charging process [5,6,21,24,25].

The thermal stability of the battery is closely related to charge state of the battery. This work focuses on the thermal stability of NMC811/Si@C battery by combining both scanning calorimetry (DSC) and adiabatic rate calorimetry (ARC). The DSC analyzes the thermal stability of battery materials with different states of charge (SOCs). The batteries are charged to different charge states with 1C current before ARC experiments. By comparing the DSC data of the electrolytes involved, the decomposition of electrode material and its reaction with the electrolyte as well as the thermal stability of battery materials at different SOCs can be more clearly observed and understood. The thermal stability mutation of the Si@C electrode material was clearly observed in DSC result. Based on the complete thermal analysis of the battery (including electrolyte, separator), a reasonable sequence of thermal runaway reactions is proposed. In addition, using the ARC data of different charge state battery, the TMR curve is predicted.

2. Experiment

2.1. DSC experiment

The experiment material was the 57 Ah NMC-811/Si@C electrode pieces taken from the battery made by JEVE. The capacity of positive electrode is 236.25 mAh·g^{-1}, which measured under the condition of constant current discharge and the cut-off voltage is 3–4.3 V. the capacity of negative electrode is 452.51 mAh·g^{-1}, which measured under the condition of constant current discharge and the cut-off voltage is 0.01–2 V. All the values above were measured from coin cells, whose electrodes are cut from the fresh commercial electrodes. The counter electrode is lithium metal. After disassembling the fresh battery, the electrode was dried, and then cut to make a 3.2 cm × 3.2 cm electrode. Next, the electrolyte was injected into the battery for charging by reassembly. The electrolyte solvent supplied by CAPCHEM consisted of EC/PC/DMC, and the solute was $LiPF_6$, in addition, additives was added to the electrolyte in order to make the battery work excellent.

The DSC experiments were conducted on the electrode materials with 5 different SOCs: 0%, 25%, 50%, 75%, and 100%. By comparing the charging curve of the battery under 1C in Fig. 1, the corresponding voltages under different SOCs were obtained and shown in Table 1:

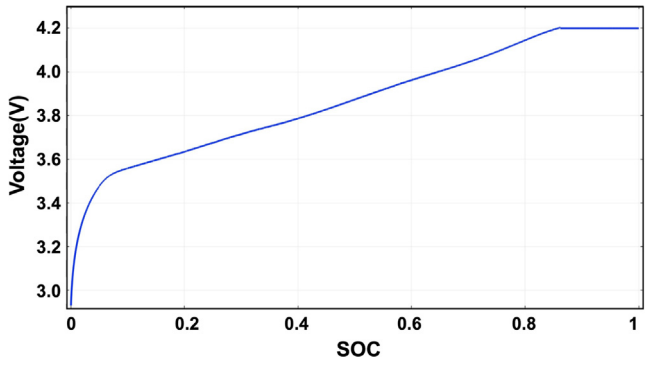

Fig. 1. Charge curve of 57 Ah lithium ion battery.

Table 1
The potential of different SOCs.

SOC	0%	25%	50%	75%	100%
Potential (V)	2.75	3.67	3.87	4.09	4.20

After the batteries were charged to the corresponding voltages in Table 1, they were quickly disassembled in the argon-filled glove-box. The electrodes were immediately washed with dimethyl carbonate (DMC), and soaked for two hours to remove the electrolyte on the electrode surface, followed by placing in the glove box for two hours to ensure there was no electrolyte residue inside the electrode material.

When the DSC experiments were carried out, the cathode and anode electrode material powders of different charge states were scratched from the electrodes with a ceramic knife, and the mass of the powders was controlled within the range of 3–10 mg. When the mass was less than 3 mg, the exothermal peaks were difficult to detect because of low heat generation. When the mass was more than 10 mg, the sealed crucible might leak due to the internal pressure increases caused by the increase of oxygen released from the cathode electrode material. The sample is prepared based on the following ratio: electrode material: electrolyte = 1 mg: 1 ul. Therefore, this operation was used to control the accuracy of the experiments. The crucible used in the DSC experiment was a gold-plated stainless steel sealed crucible. The DSC samples were prepared by adding electrolyte to electrode materials on specific ratios.

The DSC measurements were performed with a Netzsch (STA 449 F3 Jupiter®) DSC 204 (Germany). The heating rate is 5 K·min^{-1}, and test temperature range from 50 °C to 350 °C.

In addition to test the DSC data of the cathode and anode materials, the experiments also tested the electrolyte and the separator used in the 57 Ah NMC-811/Si@C pouch battery. The separator used in the pouch battery was a ceramic separator. Considering the separator melt, the DSC test temperature range from 50 °C to 200 °C. Besides, the electrodes were examined with a Rigaku Miniflex 600 X-ray diffractometer with nickel-filtered Cu Kα radiation at a scan rate of 4° per second over a 2θ range.

2.2. ARC experiment

The ARC measurements were performed with a HEL PHITEC BTC 500 (British).

The batteries used in ARC test were the research batteries made by JEVE. The batteries were charged to different SOCs at 1C (57 A) current before ARC experiments. During the heat-wait process, the sample was heated to 25 °C initially, followed by a 40 min temperature calibration. Then the sample temperature ramped up. A 30 min search process was conducted after every 5 °C ramps at 2 °C·min^{-1}. When the instrument detected the temperature of the battery rise rate exceeds 0.02 °C·min^{-1}, the program will assume that the battery has enter the self-heating process and enter a track mode. Then the ARC tracked the temperature change of the battery under an adiabatic condition. Two temperature probes were attached on the battery to detect temperature change of the battery.

Before ARC testing, thermocouples (temperature probe) were fixed to the surface at the center of the battery, and then winded the heater on the surface of the battery. Before placing the battery inside the calorimeter, the sample should be wrapped tightly by the sample heater with thermal tape as shown in Fig. S1. The batteries tested for ARC was placed on a tripod inside of the equipment. Because of the tripod's mass is too small comparing with the battery, we assume that it has no effect on the test results. There atmosphere is air used in the ARC. Besides, the dimensions of the battery for ARC test is shown in Table 2.

Table 2
The dimensions of the battery.

Capacity (Ah)	Length (mm)	Width (mm)	Thickness (mm)	Weight (g)
57	264	92	12	754 ± 3

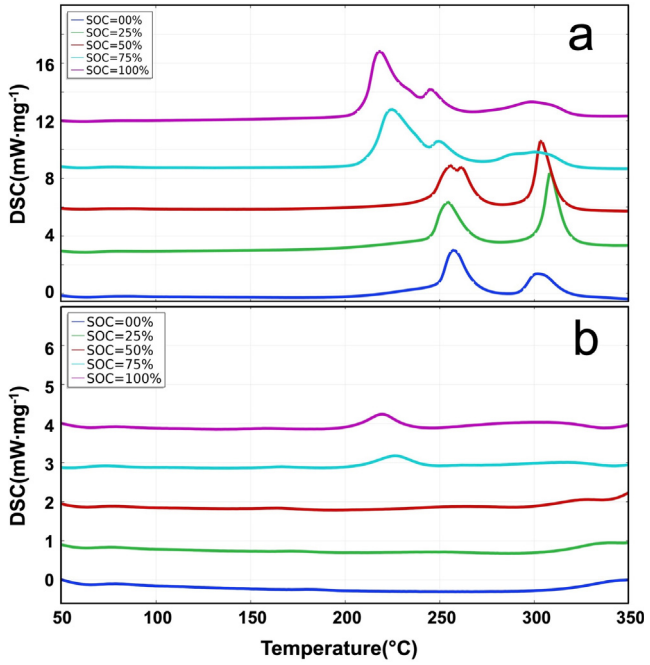

Fig. 2. DSC results of different SOC cathode. (a) Is the DSC result of cathode with electrolyte. (b) Is the DSC result of cathode without electrolyte.

3. Results and discussion

3.1. Data and analysis

3.1.1. Experiments of cathode materials

By comparing the DSC data of the cathode materials with electrolyte under different SOCs in Fig. 2(a), it can be found that there are roughly two exothermic peaks in the reaction of the cathode electrode material and the electrolyte, and the positions are around 260 °C and 310 °C. The positions of two exothermic peaks are consistent with Patrick's research [26]. According to Patrick's DSC measurements, the exothermic peaks of more than 150 °C are the cathode-electrolyte reactions [26]. As the SOCs increase, the positions of these two peaks tend to move forward. As the SOCs increased from 0% to 50%, the position of exothermic peaks remains unchanged, but the intensity of the peak at around 310 °C increased. This change also is consistent with the Patrick's research. At the same time, when SOC reaches 50%, it can be observed that the reaction peak at 260 °C is split from a single peak to double peaks. The splitting phenomenon indicted there have two or more reactions in the corresponding temperature. When the charge state changed, the reactions will change simultaneously. Different reactions have different activation energy and different reaction rate, the DSC result also can show reaction rate. Thus, the splitting phenomenon can to be understand that there have reactions happening in advance. This is a bad signal for battery safety, indicating that the self-heating reaction occurs in advance. When the SOCs are increased from 50% to 100%, the reaction peak around 260 °C will move forward, and the splitting phenomenon is more obvious. However, the reaction peak around 310 °C will gradually weaken, which is different with the change of SOCs from 0% to 50%.

Through the DSC data of the cathode electrode material without electrolyte additional reaction in Fig. 2(b), it can be inferred that the decomposition reaction peak of the cathode electrode will increase with the increase of SOCs. For the DSC data of SOCs reach 75% and 100% shown in Fig. 2(b), the reaction peak at about 230 °C should be attributed to the reaction of cathode electrode material decomposition. As the SOCs increase, the decomposition reaction peak of the NMC material gradually increases, which is similar to the Röder's research [27]. Compared with Fig. 2(a), the reaction peaks at other positions should be the peaks of the reactions of the cathode electrode material and the electrolyte. It can be inferred that the thermal decomposition of the cathode electrode material is preceded by the reaction of the cathode electrode material and the electrolyte when the battery occurred thermal runaway reaction.

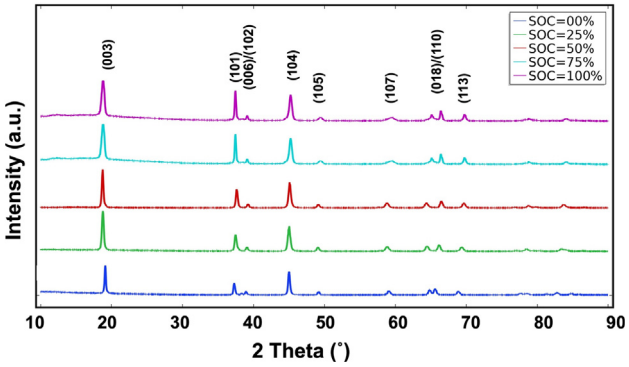

Fig. 3. XRD patterns of different charge state of cathode material.

Fig. 3 shows the powder XRD of lithium-rich NMC811 material. As the SOCs increase, the clear splitting of (0 0 6)/(1 0 2) peak will disappear first and then appear. As the SOCs increase, the clear splitting of (0 1 8)/(1 1 0) peak will firstly strengthen and then weaken. The (0 1 8) peak will move to a lower angle and then move to a higher angle, while the (1 1 0) peak changes in the opposite direction. In addition, with the continuous reduction of lithium in the cathode material, the intensity of the peak of (1 0 1) increases gradually. Combined with the DSC data, it can be seen that the thermal stability of the NMC811 material is continuously weakened when that change occurred. In particularly, the thermal stability of the NMC811 material will undergo a relatively large change when the (0 1 8) peak shifts to the right and the (1 1 0) peak shifts to a lower angle. The reason of thermal stability of NMC material will have great change when the SOCs reached 50% can be attached to the unit-cell volume change of NMC811. The unit-cell volume change can according to the change of lattice parameter *C* when the material was charged to high voltage [28]. The lattice parameter *C* will increase at the early of charge and decrease when reached the high voltage [29]. Aleksandr et al. [30] also consider that the *C* parameter for NMC811 cathode material will change when the state of charge is around 50%. When the unit-cell volume change, the surface of the material structure will crack due to stress changes, and the surface reaction is more sensitive.

3.1.2. Experiments of anode materials

From the DSC data of the reaction of the anode electrode material and the electrolyte in Fig. 4(a), it can be found that when the SOCs are increased from 0% to 50%, the intensity of the reaction peak at about 110 °C increase, and a new peak appeared at around 230 °C. When the SOCs are higher than 50%, the position of the peak will change, the reaction peak at 110 °C disappear, the peak at around 230 °C will increase, and a new peak will appear around 330 °C, and the intensity of the reaction peak will also increase.

Compared to the anode electrode material DSC data without electrolyte in Fig. 4(b), it can be found that the reaction peak at about 330 °C should be attributed to the reaction of the anode electrode material thermal decomposition, and the previous reaction peaks in

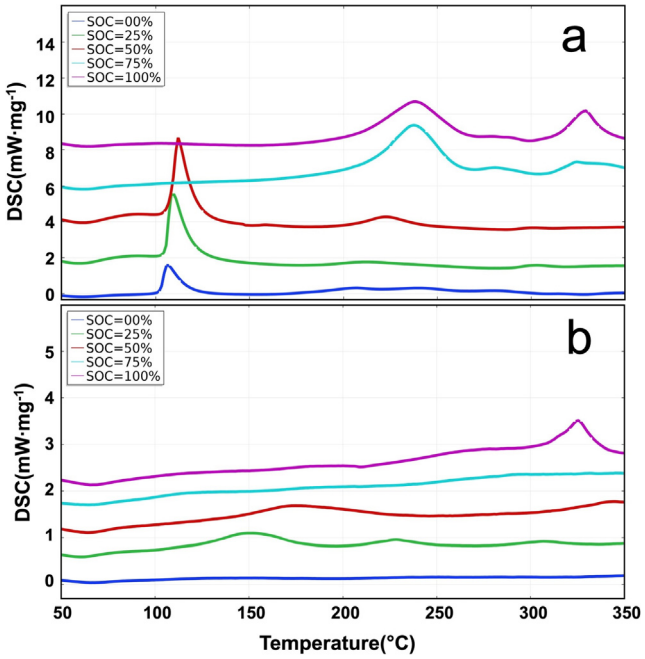

Fig. 4. DSC results of different SOC anode. (a) Is the DSC result of anode with electrolyte. (b) Is the DSC result of anode without electrolyte.

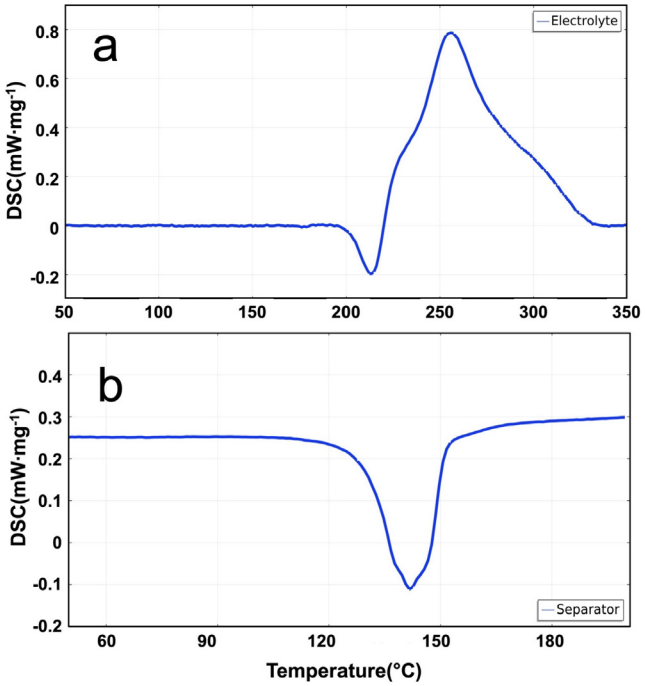

Fig. 6. (a) Is the DSC results of the electrolyte. (b) Is the DSC result of the separator.

Fig. 4(a) are attributed to the reaction of anode electrode material and the electrolyte. It can be inferred that when the anode electrode material undergoes a thermal runaway reaction, the lithium-intercalated anode electrode material will react with the electrolyte before the reaction of anode material decomposition, which is different from the reaction of cathode. Compared with the DSC data of the cathode electrode material in Fig. 2, it can be found that the heat generated by the reaction of the cathode electrode materials and the electrolyte is higher than that of the anode electrode material.

The thermal stability of the anode material will cause a large change when the SOC is greater than 50%. To find the reason, the battery research with SOC between 50% and 75% was added. From the DSC data in Fig. S2, it can be clearly seen that the exothermic peak at around 110 °C will disappear, but the exothermic peak at around 230 °C will appear when the SOC higher than 55%. Besides, compared with the DSC data of SOC equaling to 50%, it can also be found that the intensity of exothermal peak at around 110 °C has decreased but the peak at around 230 °C has increased when the SOC equal to 55%.

Fig. 5 shows the powder XRD of Si@C material. The patterns are similar to the Si@C patterns of Zhou et al. [31]. It will be found that the peak of carbon (C) element (at around 26.4°) changes with the SOCs increasing. It can be seen that the intensity of C peak will decrease when the SOC above 50%. The potential of alloying reaction with silicon during the charge process is 0.3 V, which is higher than the potential of the lithium insertion into graphite (0.1 V), so the alloying reaction with silicon will go before the lithium insertion into graphite during the charge process. The exothermal peak at around 110 °C should be the lithium intercalated silicon react with the electrolyte. Silicon, no matter crystalline or amorphous, will be transformed to an amorphous phase and subsequently transform to a crystalline compound during the lithium intercalation process [32–35]. The thermal stability of anode material change when the SOC higher than 55% should be attributed to the silicon phase change.

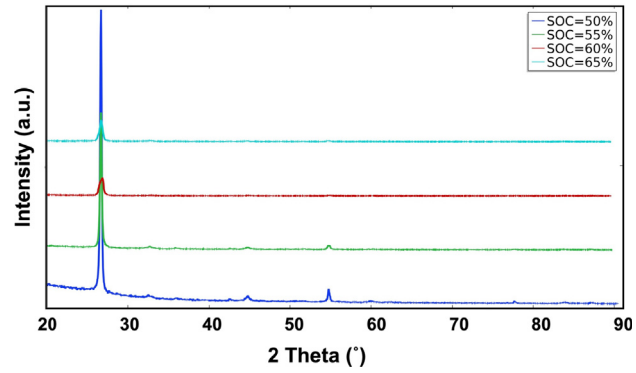

Fig. 5. XRD patterns of anode material.

3.1.3. DSC experiment of separator and electrolyte

The DSC data of the electrolyte has been obtained, and the all reaction peaks include one endothermic peaks and one exothermic peak as shown in Fig. 6(a). It can be seen that the temperature increases from 50 °C to 200 °C, the endothermic peak began at 200 °C, this reaction should be the dissolution of electrolyte salt, but at about 210 °C, the endothermic peak of the electrolyte is weakened, indicating that the electrolyte will start to heat up and liberate heat, reaching a peak at around 255 °C. According to the research of Tsukasaki et al. [36], it can be inferred that the exothermic peak at 255 °C should be the derived from $LiPF_6$ decomposition.

Observing the DSC data of the separator in Fig. 6(b), it can be found that the separator has an obvious endothermic peak around 142 °C. It can be inferred that the reaction peak should be the melting reaction peak of the separator. Compared with the traditional PE separators, the ceramic separators have a relatively small shrinkage rate under high temperature conditions [37–39].

3.2. ARC data and analysis

3.2.1. Thermal runaway temperature

Through the temperature data of the ARC experiment of the battery in Fig. 7(a), it can be found that the NMC811/Si@C batteries start self-heating at around 60 °C, and the batteries start to slowly heat up under the action of self-heating, and the heating rate as shown in Fig. 7(b). When the batteries are heated to about 100 °C, the self-heating rate of

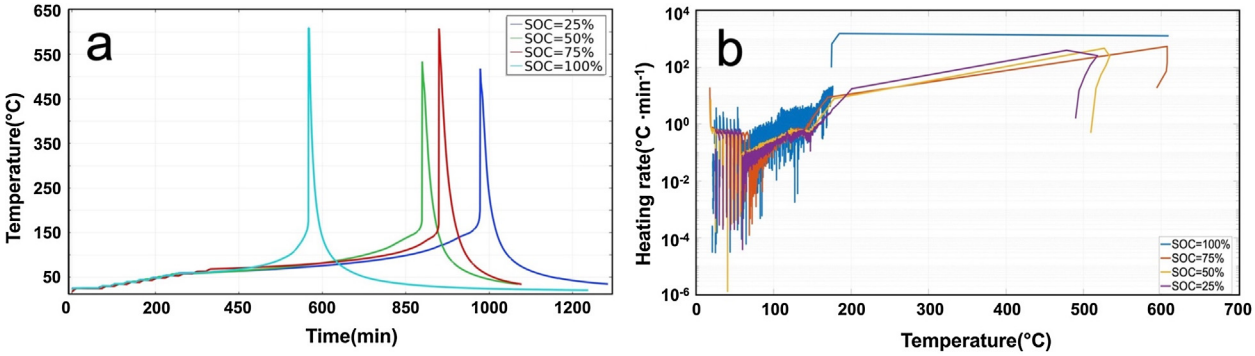

Fig. 7. Thermal runaway data. (a) Is the temperature change during the thermal runaway. (b) Is the heating rate of thermal runaway.

the battery increases, and the heating rate is about 10^{-1} °C·min^{-1}, causing the battery to continue to heat up, and heating up to 150 °C in a relatively short period of time, which causes the battery to run out of control. The batteries' temperature rises rapidly when the batteries get to 150 °C, the maximum heating rate is 10^{2} °C·min^{-1}. The maximum temperature of the thermal runaway batteries could reach more than 500 °C.

From the above, it can be concluded that the NMC811/Si@C battery will undergo thermal runaway when it reaches 150 °C, whether it is fully charged or not. It can be considered that the separator of the battery has completely melted at this temperature. Liu et al. [11] also prove that the battery can prevent thermal runaway before a certain temperature. When the temperature of the battery reaches 150 °C, the battery rapidly heats up due to its own heat generation, and the thermal runaway reaction cannot be prevented at this temperature. It can be found that the self-heating time of the lithium ion battery with the SOC reaching 75% is longer than other charging-state lithium ion batteries. But regardless of the charging state of the lithium ion battery, the temperature at the start of thermal runaway of the lithium ion battery is almost the same. Therefore, it can be recommended that in order to avoid thermal runaway of the battery, the use temperature of the battery needs to be lower than 150 °C. In order to use the battery safer, the temperature of the battery should be lower than 60 °C. The temperatures mentioned above should be lower especially when the lithium ion battery is fully charged (see Table 3).

In addition, according to the DSC data, when the states of charge increase, the reaction temperature of the anode electrode with the electrolyte increases, and the reaction temperature of the cathode electrode with the electrolyte decreases. It can be believed that when the state of charge reaches to 75%, the two reactions will occur at nearly the same temperature, and the energy released from the thermal runaway is more concentrated. Therefore, in the ARC experiment, compared with the thermal runaway data of the battery whose SOC equals to 50%, the self-heating time of the battery which SOC equals to 75% will be prolonged, but the maximum temperature of the thermal runaway will be higher.

3.2.2. Time to maximum rate

There are three important temperature parameters in the thermal runaway reaction of the battery:

Table 3
The ARC test data.

SOC	Self-heat temperature (°C)	Max-rate temperature (°C)	Max temperature (°C)
25%	59.3	148.1	517.9
50%	56.6	146.5	533.6
75%	63.1	138.8	607.8
100%	58.60	154.2	609.6

(i) The battery self-heating start temperature T_{ini}. When the battery reaches this temperature, it indicates that the battery is starting to get dangerous.
(ii) The maximum heating rate start temperature T_{fin}. This temperature is the safe threshold for the battery. When the battery temperature is higher than this value, it indicates that the irreversible thermal runaway will occur. The thermal runaway of lithium ion battery may bring great harm to human who using it.
(iii) The maximum temperature T_{max} reached by thermal runaway. This temperature indicates that the danger degree of the accident caused by thermal runaway. The higher the temperature of the lithium ion battery, the more dangerous in usually.

In the adiabatic system, the heat generated by the battery itself was completely used for the temperature rise of the sample. Assuming that the reaction equation in the thermal runaway reaction conforms to the Arrhenius equation, the following equation can be obtained by establishing the heat balance equation:

$$\frac{dT}{dt} = \frac{Q}{C_p} * A * C^n * e^{-\frac{E}{RT}} \tag{1}$$

wherein T is the reaction temperature, C is sample mass, Q is reaction heat evolution, C_p is average heat capacity of the sample, A is a factor before reaction, n is reaction order, and E is reaction activation energy.

Assuming C_p and Q are independent of sample state and temperature, it can get:

$$\frac{C_p}{Q} = \frac{C_0}{T_{max} - T_0} \tag{2}$$

where T_0 is the inital temperature of the battery.

Assuming that the sample mass C has the following relationship with the temperature T:

$$C = \frac{T_{max} - T}{T_{max} - T_0} * C_0 \tag{3}$$

By combining Eqs. (1)–(3), the self-heating thermal reaction rate of the battery sample can be obtained as following:

$$\frac{dT}{dt} = A * \left(\frac{T_{max} - T}{T_{max} - T_0}\right)^n * (T_{max} - T_0) * {C_0}^n * e^{-\frac{E}{RT}} \tag{4}$$

Eq. (4) is used to fit the thermal runaway temperature data of the lithium ion batteries. Assuming a value of the reaction order number, the reaction pre-factor and activation energy of the thermal runaway reaction can be obtained.

The time to maximum rate (TMR) represents the time required to reach the maximum reaction rate, also is the time before thermal runaway occur in this temperature. The TMR can get from Eq. (5) [40]:

$$TMR = \frac{R * T^2}{\frac{dT}{dt} * E} \tag{5}$$

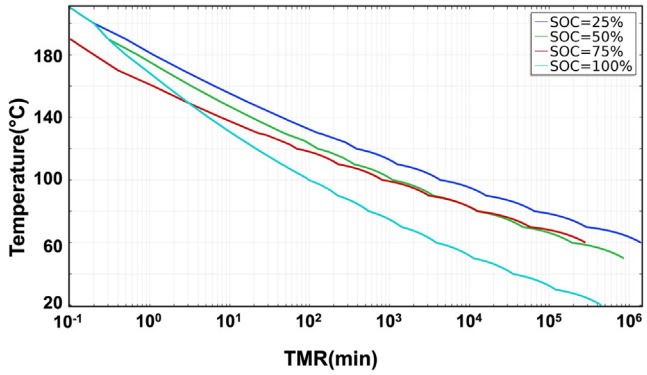

Fig. 8. TMR of different charge state batteries.

Using the above method to analyze the NMC811/Si@C battery, and assuming the reaction order number $n = 2$, the TMR data can be obtained, as shown in Fig. 8. It can be seen directly that as the temperature increases, the TMR will become smaller and smaller, indicating that the higher the temperature, the lower the thermal stability of the battery. For example, according to Fig. 8, the battery with full charged reaches the maximum reaction rate after 24 h at 77.9 °C, that is, the thermal runaway occurs. At 88.6 °C, the reaction rate will reach a maximum reaction rate after 8 h. However, the battery with the SOC equaling to 75% can reach a maximum reaction rate at 95.7 °C for 24 h. It can get a conclusion from Fig. 8 that, compared with other charge state batteries, the NMC811/Si@C lithium ion battery whose SOC equals to 75% can be safely stored for a longer time in higher temperature environment. But the separator will melt at high environment, the battery will absolutely thermal runaway due to internal short.

3.2.3. Battery after ARC pictures

By observing the photos after the thermal runaway of the battery in Fig. S3, it can be found that the integrity of the battery after the ARC experiment decreases with the increase of the state of charge. After the battery thermal runaway, the battery of SOC 25% can only maintain its original shape better mostly in Fig. S3. The battery with SOCs reaching to 75% and 100% experiments have completely turned into pieces. It was known that although the battery of SOC equaling to 75% can maintain relatively good thermal stability, but the internal energy is relatively large, the damage of battery of SOC equaling to 75% caused by thermal runaway is still relatively large. So the integrity of battery after the ARC experiment is relative with the energy stored.

When observing the sample after the thermal runaway of the battery, it was found that after the battery of different charge states was out of control, the cathode current collector was not seen, but the anode current collector could be found. However, as the states of charge increasing, the integrity of the anode current collector continues to decrease. Silver-white particles were found in the battery residue. In addition, golden yellow particles were found in the battery of SOCs equaling to 50%, 75%, and 100% residues, and the radius of the particles also increased with the increase of SOCs. It was suspected that the silver-white particles were the product of the melting of the cathode current collector, and the gold-yellow particles were the product of the melting of the anode current collector.

Here are some speculations about the possibility of thermite reaction inside the battery. The classical thermite reaction is the reaction of iron oxide and aluminum. The NMC811 material is also a metal oxide, and the current collector of the cathode electrode is aluminum foil, and the two are in close contact. In the event of thermal runaway, the pressure inside the battery can be as high as 5–10 bar [26], besides, the thickness of the cathode current collector is only 13 μm. Under this condition, a thermite reaction may occur. There are some related literatures that report the thermite reaction inside the battery [41–43]. Based on the above analysis, it was believed that the thermite reaction is likely to occur at the moment when the battery thermal runaway, therefore, the silvery white particles may be formed by the thermite reaction, and due to the thermite reaction temperature, golden yellow particles may be the melted copper.

Based on the above DSC data analysis and ARC data analysis, it can be inferred that the internal reaction sequence in the NMC811/Si@C battery thermal runaway should be as follows: First, the Solid Electrolyte Layer (SEI) on the anode electrode surface liberates heated at the temperature about 60–110 °C [44–46], this point can also be confirmed in Fig. 7 that the self-heat temperature of battery thermal runaway starts at about the temperature of 60 °C. But this part of the reaction heat is small [47], hence the temperature rise rate of the battery is relatively slow at the start of exothermic process. Next, the anode electrode reacts with the electrolyte. Because the battery reacts at different SOCs, the exothermic is different in the reaction of different SOCs anode with electrolyte. Therefore, this is also the reason why the self-heating rate of the different state of charge cells is inconsistent after the self-heating is reached. When the battery temperature reaches 110 °C, the reaction rate reaches the maximum, causing a significant increase in the temperature rise rate of the battery as shown in Fig. 7. When the battery temperature rises to 142 °C, the melting separator may cause the internal short circuit, because electrical energy was converted into heat, so the internal short circuit will cause the temperature of the battery to rise linearly. The reaction that occurs afterwards will be the decomposition of cathode material, followed by the reaction of the electrolyte with the cathode material, which will make the temperature rise sharply because the exothermal in this step is bigger than other reactions.

There are two reasons for the difference in the maximum average temperature of the thermal runaway temperature of different rechargeable batteries. One is that the battery is in a different state of charge, and the energy released by the internal short circuit is different, hence the amount of heat converted is also different. The other is that the exothermic amount of the decomposition reaction is different from the reaction of electrolytes with cathode materials. The heat released by the reaction of the anode electrode initiates the self-heating of the battery, but the heat generated by the reaction of the cathode electrode material triggers thermal runaway and contributes to the maximum temperature of thermal runaway, which is also the most direct cause of battery explosion.

4. Conclusion

By performing both DSC experiments and ARC experiments on the NMC811/Si@C battery materials and the pouch batteries, it can be found that when the SOC is more than 50%, the reaction of the cathode and anode materials will undergo a relatively large change. When the batteries are at different SOCs, the self-heating start temperature and the thermal runaway trigger temperature do not change greatly. The NMC811/Si@C battery will start to self-heat at around 60 °C, and the thermal runaway will occur at 150 °C. So the battery use temperature can refer to those values.

The significance of this work is to provide recommendations for better and safer use of batteries based on both ARC and TMR data.

Acknowledgements

We gratefully acknowledge the financial support of National Key Research and Development Program of China (2017YFB0102000, 2017YFB0102003), National Natural Science Foundation of China (21603179, 21621091), the Fundamental Research Funds for the Central Universities (20720170021).

Appendix A. Supplementary material

Supplementary data to this article can be found online at https://

doi.org/10.1016/j.applthermaleng.2019.114144.

References

[1] Z.P. Cano, D. Banham, S. Ye, A. Hintennach, J. Lu, M. Fowler, et al., Batteries and fuel cells for emerging electric vehicle markets, Nat. Energy 3 (2018) 279–289, https://doi.org/10.1038/s41560-018-0108-1.

[2] R. Schmuch, R. Wagner, G. Hörpel, T. Placke, M. Winter, Performance and cost of materials for lithium-based rechargeable automotive batteries, Nat. Energy 3 (2018) 267–278, https://doi.org/10.1038/s41560-018-0107-2.

[3] E.C. Evarts, Researchers are developing a type of battery that has ten times the power of conventional batteries, vol. 3, n.d.

[4] R.V. Noorden, Chemists are reinventing rechargeable cells to drive down costs and boost capacity, vol. 3, n.d.

[5] J.-Y. Li, Q. Xu, G. Li, Y.-X. Yin, L.-J. Wan, Y.-G. Guo, Research progress regarding Si-based anode materials towards practical application in high energy density Li-ion batteries, Mater. Chem. Front. 1 (2017) 1691–1708, https://doi.org/10.1039/C6QM00302H.

[6] D. Ma, Z. Cao, A. Hu, Si-based anode materials for Li-ion batteries: a mini review, Nano-Micro. Lett. 6 (2014) 347–358, https://doi.org/10.1007/s40820-014-0008-2.

[7] L. Zhang, X. Liu, Q. Zhao, S. Dou, H. Liu, Y. Huang, et al., Si-containing precursors for Si-based anode materials of Li-ion batteries: a review, Energy Stor. Mater. 4 (2016) 92–102, https://doi.org/10.1016/j.ensm.2016.01.011.

[8] L. Su, Z. Zhou, M. Ren, Core double-shell Si@SiO_2@C nanocomposites as anode materials for Li-ion batteries, Chem. Commun. 46 (2010) 2590, https://doi.org/10.1039/b925696b.

[9] J. Sturm, A. Rheinfeld, I. Zilberman, F.B. Spingler, S. Kosch, F. Frie, et al., Modeling and simulation of inhomogeneities in a 18650 nickel-rich, silicon-graphite lithium-ion cell during fast charging, J. Pow. Sour. 412 (2019) 204–223, https://doi.org/10.1016/j.jpowsour.2018.11.043.

[10] L. Visser, Y. Gao, Stabilized NMC811 to enable high energy density lithium ion batteries, vol. 28, n.d.

[11] X. Liu, D. Ren, H. Hsu, X. Feng, G.-L. Xu, M. Zhuang, et al., Thermal runaway of lithium-ion batteries without internal short circuit, Joule (2018), https://doi.org/10.1016/j.joule.2018.06.015.

[12] T.-H. Kim, J.-S. Park, S.K. Chang, S. Choi, J.H. Ryu, H.-K. Song, The current move of lithium ion batteries towards the next phase, Adv. Energy Mater. 2 (2012) 860–872, https://doi.org/10.1002/aenm.201200028.

[13] R. Jung, R. Morasch, P. Karayaylali, K. Phillips, F. Maglia, C. Stinner, et al., Effect of ambient storage on the degradation of Ni-rich positive electrode materials (NMC811) for Li-ion batteries, J. Electroch. Soc. 165 (2018) A132–A141, https://doi.org/10.1149/2.0401802jes.

[14] R. Jung, M. Metzger, F. Maglia, C. Stinner, H.A. Gasteiger, Chemical versus electrochemical electrolyte oxidation on NMC111, NMC622, NMC811, LNMO, and conductive carbon, J. Phys. Chem. Lett. 8 (2017) 4820–4825, https://doi.org/10.1021/acs.jpclett.7b01927.

[15] S.-M. Bak, E. Hu, Y. Zhou, X. Yu, S.D. Senanayake, S.-J. Cho, et al., Structural changes and thermal stability of charged $LiNi_xMn_yCo_zO_2$ cathode materials studied by combined *In Situ* time-resolved XRD and mass spectroscopy, ACS Appl. Mater. Inter. 6 (2014) 22594–22601, https://doi.org/10.1021/am506712c.

[16] I. Belharouak, W. Lu, D. Vissers, K. Amine, Safety characteristics of Li$(Ni_{0.8}Co_{0.15}Al_{0.05})O_2$ and Li$(Ni_{1/3}Co_{1/3}Mn_{1/3})O_2$, Electroch. Commun. 8 (2006) 329–335, https://doi.org/10.1016/j.elecom.2005.12.007.

[17] Z. Liu, Q. Yu, Y. Zhao, R. He, M. Xu, S. Feng, et al., Silicon oxides: a promising family of anode materials for lithium-ion batteries, Chem. Soc. Rev. 48 (2019) 285–309, https://doi.org/10.1039/C8CS00441B.

[18] H.S. Choi, J.G. Lee, H.Y. Lee, S.W. Kim, C.R. Park, Effects of surrounding confinements of Si nanoparticles on Si-based anode performance for lithium ion batteries, Electrochim. Acta. 56 (2010) 790–796, https://doi.org/10.1016/j.electacta.2010.09.101.

[19] P. Li, G. Zhao, X. Zheng, X. Xu, C. Yao, W. Sun, et al., Recent progress on silicon-based anode materials for practical lithium-ion battery applications, Energy Stor. Mater. 15 (2018) 422–446, https://doi.org/10.1016/j.ensm.2018.07.014.

[20] X. Zuo, J. Zhu, P. Müller-Buschbaum, Y.-J. Cheng, Silicon based lithium-ion battery anodes: a chronicle perspective review, Nano Energy 31 (2017) 113–143, https://doi.org/10.1016/j.nanoen.2016.11.013.

[21] R. Hu, W. Sun, Y. Chen, M. Zeng, M. Zhu, Silicon/graphene based nanocomposite anode: large-scale production and stable high capacity for lithium ion batteries, J. Mater. Chem. A 2 (2014) 9118–9125, https://doi.org/10.1039/C4TA01013B.

[22] C.K. Chan, R. Ruffo, S.S. Hong, Y. Cui, Surface chemistry and morphology of the solid electrolyte interphase on silicon nanowire lithium-ion battery anodes, J. Power Sourc. 189 (2009) 1132–1140, https://doi.org/10.1016/j.jpowsour.2009.01.007.

[23] Y. Oumellal, N. Delpuech, D. Mazouzi, N. Dupré, J. Gaubicher, P. Moreau, et al., The failure mechanism of nano-sized Si-based negative electrodes for lithium ion batteries, J. Mater. Chem. 21 (2011) 6201, https://doi.org/10.1039/c1jm10213c.

[24] H. Wu, Y. Cui, Designing nanostructured Si anodes for high energy lithium ion batteries, Nano Today 7 (2012) 414–429, https://doi.org/10.1016/j.nantod.2012.08.004.

[25] M.K. Jangid, S. Sinha, A.S. Lakhnot, F.J. Sonia, A. Kumar, R.O. Dusane, et al., Effect of the presence of Si-oxide/sub-oxide surface layer(s) on 'micron-sized' Si wires towards the electrochemical behavior as anode material for Li-ion battery, Electrochim. Acta. 297 (2019) 381–391, https://doi.org/10.1016/j.electacta.2018.11.201.

[26] P. Röder, B. Stiaszny, J.C. Ziegler, N. Baba, P. Lagaly, H.-D. Wiemhöfer, The impact of calendar aging on the thermal stability of a $LiMn_2O_4$–Li$(Ni_{1/3}Mn_{1/3}Co_{1/3})O_2$/graphite lithium-ion cell, J. Pow. Sourc. 268 (2014) 315–325, https://doi.org/10.1016/j.jpowsour.2014.06.040.

[27] P. Röder, N. Baba, H.-D. Wiemhöfer, A detailed thermal study of a Li$[Ni_{0.33}Co_{0.33}Mn_{0.33}]O_2$/$LiMn_2O_4$-based lithium ion cell by accelerating rate and differential scanning calorimetry, J. Pow. Sourc. 248 (2014) 978–987, https://doi.org/10.1016/j.jpowsour.2013.09.146.

[28] A.O. Kondrakov, A. Schmidt, J. Xu, H. Geßwein, R. Mönig, P. Hartmann, et al., Anisotropic lattice strain and mechanical degradation of high- and low-nickel NCM cathode materials for Li-Ion batteries, J. Phys. Chem. C 121 (2017) 3286–3294, https://doi.org/10.1021/acs.jpcc.6b12885.

[29] S.-W. Lee, D.-H. Jang, J.-B. Yoon, Y.-H. Cho, Y.-S. Lee, D.-H. Kim, et al., Crystal structure changes of $LiNi_{0.5}Co_{0.2}Mn_{0.3}O_2$ cathode materials during the first charge investigated by in situ XRD, J. Electroch. Sci. Technol. 3 (2012) 29–34, https://doi.org/10.33961/JECST.2012.3.1.29.

[30] A.O. Kondrakov, H. Geßwein, K. Galdina, L. de Biasi, V. Meded, E.O. Filatova, et al., Charge-transfer-induced lattice collapse in Ni-Rich NCM cathode materials during delithiation, J. Phys. Chem. C 121 (2017) 24381–24388, https://doi.org/10.1021/acs.jpcc.7b06598.

[31] R. Zhou, R. Fan, Z. Tian, Y. Zhou, H. Guo, L. Kou, et al., Preparation and characterization of core–shell structure Si/C composite with multiple carbon phases as anode materials for lithium ion batteries, J. Alloys. Compd. 658 (2016) 91–97, https://doi.org/10.1016/j.jallcom.2015.10.217.

[32] J. Li, J.R. Dahn, An in situ X-ray diffraction study of the reaction of Li with crystalline Si, J. Electroch. Soc. 154 (2007) A156, https://doi.org/10.1149/1.2409862.

[33] X.H. Liu, L.Q. Zhang, L. Zhong, Y. Liu, H. Zheng, J.W. Wang, et al., Ultrafast electrochemical lithiation of individual Si nanowire anodes, Nano Lett. 11 (2011) 2251–2258, https://doi.org/10.1021/nl200412p.

[34] M.N. Obrovac, L. Christensen, Structural changes in silicon anodes during lithium insertionõextraction vol. 4, n.d.

[35] C.-M. Wang, X. Li, Z. Wang, W. Xu, J. Liu, F. Gao, et al., In situ TEM investigation of congruent phase transition and structural evolution of nanostructured silicon/carbon anode for lithium ion batteries, Nano Lett. 12 (2012) 1624–1632, https://doi.org/10.1021/nl204559u.

[36] H. Tsukasaki, W. Fukuda, H. Morimoto, T. Arai, S. Mori, A. Hayashi, et al., Thermal behavior and microstructures of cathodes for liquid electrolyte-based lithium batteries, Sci. Rep. 8 (2018), https://doi.org/10.1038/s41598-018-34017-2.

[37] J.-A. Choi, S.H. Kim, D.-W. Kim, Enhancement of thermal stability and cycling performance in lithium-ion cells through the use of ceramic-coated separators, J. Pow. Sourc. 195 (2010) 6192–6196, https://doi.org/10.1016/j.jpowsour.2009.11.020.

[38] J. Dai, C. Shi, C. Li, X. Shen, L. Peng, D. Wu, et al., A rational design of separator with substantially enhanced thermal features for lithium-ion batteries by the polydopamine–ceramic composite modification of polyolefin membranes, Energy Environ. Sci. 9 (2016) 3252–3261, https://doi.org/10.1039/C6EE01219A.

[39] C. Shi, J. Dai, X. Shen, L. Peng, C. Li, X. Wang, et al., A high-temperature stable ceramic-coated separator prepared with polyimide binder/Al_2O_3particles for lithium-ion batteries, J. Membr. Sci. 517 (2016) 91–99, https://doi.org/10.1016/j.memsci.2016.06.035.

[40] B. Roduit, P. Folly, A. Sarbach, et al., Estimation of time to maximum rate under adiabatic conditions (TMRad) using kinetic parameters derived from DSC-investigation of thermal behavior of 3-methyl-4-nitrophenol, Chem. Propel. Polym. Mater. 1 (2011) 84–93.

[41] M. Iwama, K. Abe, (54) Secondary battery (71) applicant: sony corporation, Tokyo (JP), vol. 35, n.d.

[42] S. Sriramulu, R. Stringfellow, Internal short circuits in lithium-ion cells for PHEVs, 2013. doi:10.2172/1124078.

[43] C. Mikolajczak (Ed.), Lithium-Ion Batteries Hazard and Use Assessment, Springer, New York, 2011.

[44] X. Feng, M. Ouyang, X. Liu, L. Lu, Y. Xia, X. He, Thermal runaway mechanism of lithium ion battery for electric vehicles: a review, Energy Stor. Mater. 10 (2018) 246–267, https://doi.org/10.1016/j.ensm.2017.05.013.

[45] N.E. Galushkin, N.N. Yazvinskaya, D.N. Galushkin, Mechanism of thermal runaway in lithium-ion cells, J. Electroch. Soc. 165 (2018) A1303–A1308, https://doi.org/10.1149/2.0611807jes.

[46] D. Ren, X. Liu, X. Feng, L. Lu, M. Ouyang, J. Li, et al., Model-based thermal runaway prediction of lithium-ion batteries from kinetics analysis of cell components, Appl. Energy 228 (2018) 633–644, https://doi.org/10.1016/j.apenergy.2018.06.126.

[47] M.-H. Ryou, J.-N. Lee, D.J. Lee, W.-K. Kim, Y.K. Jeong, J.W. Choi, et al., Effects of lithium salts on thermal stabilities of lithium alkyl carbonates in SEI layer, Electrochim. Acta. 83 (2012) 259–263, https://doi.org/10.1016/j.electacta.2012.08.012.